

Prediction of two-dimensional electron gas mediated magnetoelectric coupling at ferroelectric PbTiO₃/SrTiO₃ heterostructures

Lan-ying Wei,¹ Chao Lian,¹ and Sheng Meng^{1,2,*}¹*Beijing National Laboratory for Condensed Matter Physics and Institute of Physics, Chinese Academy of Sciences, Beijing, 100190, People's Republic of China*²*Collaborative Innovation Center of Quantum Matter, Beijing, 100190, People's Republic of China*

(Received 3 January 2017; revised manuscript received 30 March 2017; published 1 May 2017)

First-principles calculations predict the emergence of magnetoelectric coupling mediated by two-dimensional electron gas (2DEG) at the ferroelectric PbTiO₃/SrTiO₃ heterostructure. Free electrons endowed by naturally existing oxygen vacancies in SrTiO₃ are driven to the heterostructure interface under the polarizing field of ferroelectric PbTiO₃ to form a 2DEG. The electrons are captured by interfacial Ti atoms, which surprisingly exhibits ferromagnetism even at room temperature with a small critical density of $\sim 15.5 \mu\text{C}/\text{cm}^2$. The ferroelectricity-controlled ferromagnetism mediated by interfacial 2DEG shows strong magnetoelectric coupling strength, enabling convenient control of magnetism by electric field and vice versa. The PbTiO₃/SrTiO₃ heterostructure is cheap, easily grown, and controllable, promising future applications in low-cost spintronics and information storage at ambient condition.

DOI: [10.1103/PhysRevB.95.184102](https://doi.org/10.1103/PhysRevB.95.184102)

Traditional magnetic recording media have disadvantages of instability, slow switching speed, and high energy consumption [1]. The emergence of multiferroic materials can solve these problems to a large extent. Magnetoelectric coupling in multiferroic materials enables ferromagnetism controlled by electric field, largely reducing energy consumption and accelerating storage velocity [2]. However, ferroelectricity and ferromagnetism are always difficult to coexist, because the empty *d*-electron configurations (e.g., Ti⁴⁺) needed in ferroelectric phases obviously contradict with the partially filled *d* states required for ferromagnetism [3,4]. A single-phase ferromagnet that is also ferroelectric at room temperature has not yet been found [5]. On the other hand, one can obtain magnetoelectric coupling in heterostructures and composite materials. In recent years extensive research activities have been focused on oxide heterostructures in the hope that one-half of the interface can provide ferroelectricity and the other half provide ferromagnetism. For example, in BaTiO₃/SrRuO₃ heterostructures [6], ferroelectricity couples with magnetism in the ferromagnetic metal SrRuO₃ at the interface. In PbTiO₃/LaAlO₃ heterostructures [7], ferromagnetism could occur at ferroelectric domain walls.

The emergence of ferromagnetism in BaTiO₃/SrRuO₃ and PbTiO₃/LaAlO₃ comes from electrons trapped at the interfaces or domain walls, but whether there exists nonlocal two-dimensional electron gas (2DEG) therein is unknown. The 2DEG at low temperature is always accompanied with superconductivity, quantum Hall effect, and other complex emergent quantum behaviors. Consequently, the conductive heterointerfaces have attracted wide attention. Since the discovery of 2DEG at the interface of two insulators LaAlO₃ and SrTiO₃ [8–10], other systems that can host 2DEG have been revealed, including KNbO₃/SrTiO₃ [11], BiFeO₃/SrTiO₃ [12], etc. However, whether the 2DEG is magnetic or not, and moreover, whether there exists 2DEG-mediated magnetoelectric

coupling, are still under heavy debate for LaAlO₃/SrTiO₃ [13–15], or largely unnoticed for KNbO₃/SrTiO₃ and BiFeO₃/SrTiO₃. In addition, the interfaces of these systems are charged (e.g., in the form of LaO⁺, NbO₂⁺), and the existence of 2DEG is strongly interface composition dependent [10]; hence it is arduous to grow such samples and to control the 2DEG as well as the magnetoelectric coupling (if it exists).

Here we explore the emergence of 2DEG-mediated magnetoelectric coupling in the PbTiO₃/SrTiO₃ heterostructure. We choose this system for several reasons: (i) PbTiO₃ is a typical ferroelectric material with a strong bulk spontaneous polarization calculated to be $109.8 \mu\text{C}/\text{cm}^2$, which is 3 times larger than that of another commonly used ferroelectric material BaTiO₃. (ii) The oxygen vacancy (*V*_O) is ubiquitous and controllable in SrTiO₃, which can provide a high density of free electrons. (iii) PbTiO₃ and SrTiO₃ both have perovskite structures with the same, continuous crystal framework built by TiO₆ octahedra. The crystalline structure of the heterostructure is nondisruptive, and there is only a neutral Ti-O plane at the interface. (iv) Meanwhile, the lattice mismatch between the (001) facets of PbTiO₃ and SrTiO₃ is as small as 0.1%. It would be easy to grow a PbTiO₃/SrTiO₃ heterostructure, and the resulting heterostructure is very stable. (v) The elements in PbTiO₃/SrTiO₃ are all earth abundant; thus it is readily available and of low cost, opposite to popular systems such as LaAlO₃/SrTiO₃ and BaTiO₃/SrRuO₃ previously studied. To our surprise, we found that a 2DEG is formed at the interface of ferroelectric PbTiO₃/SrTiO₃ heterostructure upon the presence of natural defects such as *V*_O. The 2DEG exhibits ferromagnetism, even at room temperature, with a small critical density of $\sim 15.5 \mu\text{C}/\text{cm}^2$. Due to the presence of 2DEG, the calculated magnetoelectric coupling is stronger than that of BaTiO₃/SrRuO₃, and can be further modulated to larger values by increasing the density of 2DEG through increasing the density of *V*_O, applying tensile strain and/or external electric field in practice, enabling effective control of magnetism by electric field and vice versa, and facilitating future applications in low-cost spintronics and information storage at room temperature.

*smeng@iphy.ac.cn

First-principles calculations within the framework of density functional theory (DFT) are performed with VASP package [16]. We use the generalized gradient approximation (GGA) of Perdew, Burke, and Ernzerhof (PBE) [17] for the exchange-correlation functional. A projector augmented wave (PAW) [18] with electronic configurations of Pb $6s^2 6p^2$, Sr $4s^2 4p^6 5s^2$, Ti $3d^4$, O $2p^6$ is employed. The energy cutoff for plane waves is 500 eV. Because of the effects of the depolarization field, the two-dimensional PbTiO_3 thin film cannot maintain ferroelectricity [19–25], and hence we adopt $\text{PbTiO}_3/\text{SrTiO}_3$ superlattices [26] to ensure the presence of ferroelectricity at the heterointerface in the present study. The Γ -centered $2 \times 2 \times 1$ k points for $(\text{PbTiO}_3)_{2 \times 2 \times 5}/(\text{SrTiO}_3)_{2 \times 2 \times 5}$ heterostructure (periodic 2×2 supercell in the X - Y plane parallel to the interface and 5-unit-cell thickness in the perpendicular Z axis for both PbTiO_3 and SrTiO_3) and Monkhorst-Pack $5 \times 5 \times 1$ k points for $(\text{PbTiO}_3)_{1 \times 1 \times 7}/(\text{SrTiO}_3)_{1 \times 1 \times 7}$ heterostructure (periodic 1×1 supercell in the X - Y plane and 7-unit-cell thickness in the Z axis for both PbTiO_3 and SrTiO_3) are used to sample the Brillouin zone. The tolerance for total energy convergence is 10^{-4} eV. Structure relaxation is converged until the forces on all atoms are less than 0.04 eV/Å. Different lattice constants of intact neutral $\text{PbTiO}_3/\text{SrTiO}_3$ superlattice are used to simulate a strained heterostructure at the interface region with the strain $\varepsilon = \frac{a-a_0}{a_0}$, where the unconstrained ($\varepsilon = 0\%$) in-plane lattice constant is $a_0 = 3.87$ Å.

The atomic structure of the $(\text{PbTiO}_3)_{2 \times 2 \times 5}/(\text{SrTiO}_3)_{2 \times 2 \times 5}$ superlattice is shown in Fig. 1(a). Bulk PbTiO_3 and SrTiO_3 both have a cubic perovskite structure. The TiO_6 octahedra build up the crystal framework with Ti atoms located at the center of octahedra. When PbTiO_3 is deposited on the SrTiO_3 substrate, polarization of ferroelectric PbTiO_3 breaks the space-reversal symmetry of the system, driving the interfacial SrTiO_3 layers partially polarized [the case of intact structure in Fig. 1(b)]. As a result, there is a positively polarized Ti-O interface P^+ and a negatively polarized Ti-O interface P^- at the two ends of the PbTiO_3 segment: the former is the layer with polarization pointing from PbTiO_3 to SrTiO_3 , while the latter has polarization pointing from SrTiO_3 to PbTiO_3 . The two interfaces are naturally different. Here we assume the initial polarization of the system is leftward in Fig. 1.

A 2DEG arises at the P^+ interface when oxygen vacancies are present in SrTiO_3 . In experimental conditions, SrTiO_3 substrate inevitably introduces a certain amount (usually a few percent: 0.4%–10%) of oxygen vacancies in its lattice [27]. In bulk SrTiO_3 , two extra electrons introduced by each V_O localize at the vacant anionic sites; hence the adjacent Ti atoms develop a local magnetic moment of $1 \mu_B$ [28–30]. However, in the $\text{PbTiO}_3/\text{SrTiO}_3$ heterostructure, two extra electrons from a V_O in polarized SrTiO_3 are no longer localized around the local V_O site; instead, they are transferred from V_O to the positively polarized interface P^+ and become accumulated at the P^+ interface. As shown in Fig. 2(a), analysis on the partial density of states (PDOS) of Ti $3d$ orbitals shows that the conduction bands below the Fermi energy level at the sixth (P^+) and eighth atomic layers are now occupied mainly by spin-up electrons (here the spin-up charge density σ_\uparrow is about 8 times larger than that of spin-down σ_\downarrow); therefore V_O provides abundant electron doping to the interface. The free

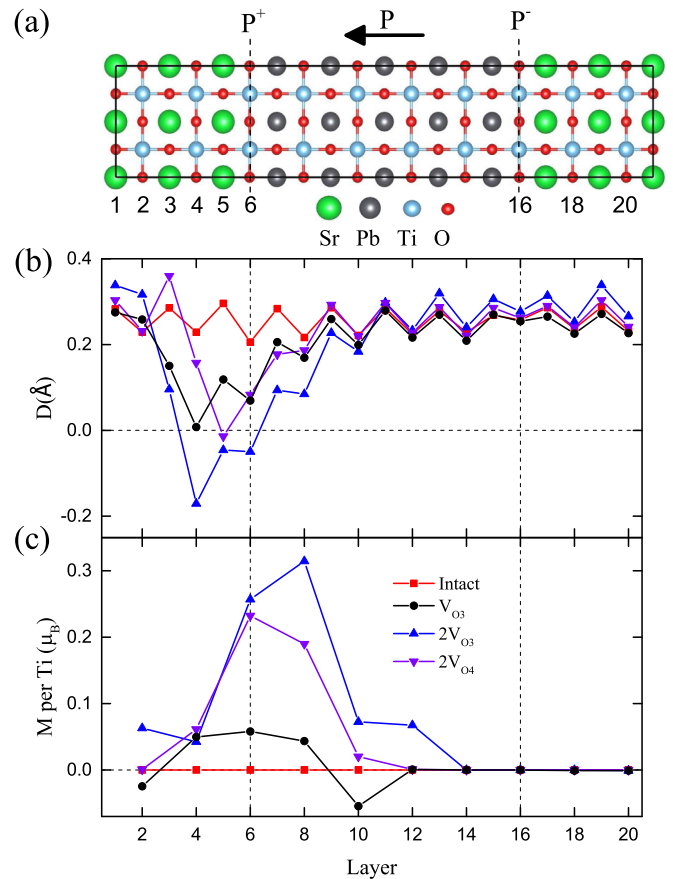


FIG. 1. (a) Atomic structure of $(\text{PbTiO}_3)_{2 \times 2 \times 5}/(\text{SrTiO}_3)_{2 \times 2 \times 5}$ superlattice. PbTiO_3 is sandwiched between SrTiO_3 layers. Vertical dashed lines denote the Ti-O interfaces. (b) The average local out-of-plane displacements between cations and anions in the same layer. (c) Layer-averaged magnetic moments per Ti atom in each Ti-O layer. V_{O3} and V_{O4} are the oxygen vacancies located at the third and fourth atomic layer (the Ti-O layer and Sr-O layer), respectively.

electrons are accumulated at the P^+ interface to form a 2DEG, and the interface becomes metallic. The 2DEG resides at the interface of the heterostructure with a small thickness of 1–2 unit cells.

In Fig. 1(c), we find that there is no magnetism present in the intact structure, but Ti atoms at the P^+ interface become ferromagnetic when V_O are added into the SrTiO_3 lattice. The ferromagnetism of Ti atoms at the P^+ interface is energetically favorable than other magnetic orderings (e.g., antiferromagnetic ordering). The shapes of spin density distribution in Fig. 2(b) indicate that the magnetism mainly comes from Ti $3d_{xz}$ and $3d_{yz}$ orbitals. Consequently, the accumulated electrons captured by interfacial Ti atoms produce ferromagnetism, resulting in magnetoelectric coupling at the interface. In the presence of V_O , the Ti atoms adjacent to V_O in the bulk SrTiO_3 and the interface Ti atoms in the $\text{PbTiO}_3/\text{SrTiO}_3$ heterostructure both exhibit ferromagnetism, but they can have different exchange interaction strengths [31]. In addition, oxygen anions around the P^+ interface are also slightly spin polarized, with the value of magnetic moment being about 1/10 of that for Ti, oriented in the opposite direction.

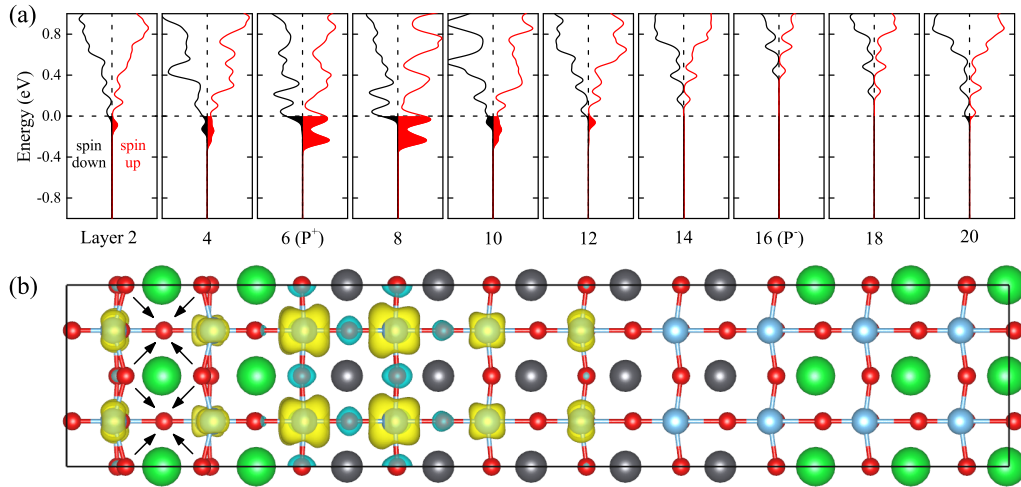


FIG. 2. Electronic properties for $2V_{O3}$ doped $(PbTiO_3)_{2 \times 2 \times 5}/(SrTiO_3)_{2 \times 2 \times 5}$. (a) The partial density of states (PDOS) of Ti $3d$ orbitals at each Ti-O layer. Red and black lines represent the contributions of spin-up and spin-down electrons, respectively. The shaded areas denote the filled energy range of conduction band bottom. (b) Spatial distribution of spin density (the difference between spin-up and spin-down charge density). The isosurface level is $\pm 0.001 e/\text{\AA}^3$ for spin-up (yellow) and spin-down (blue) electron clouds. The arrows in the left part denote adjacent oxygen anions moving toward the location of V_O .

To quantify the strength of magnetoelectric coupling, we introduce the following parameter [6]:

$$\eta = \frac{\sigma^s}{P}, \quad (1)$$

which is the ratio between the spin density σ^s at the P^+ layer and the polarization P of inner unit cell of $PbTiO_3$. Here σ^s equals to difference between spin-up and spin-down electron density, i.e., $\sigma^s = \sigma_{\uparrow} - \sigma_{\downarrow}$. The $0.058 \mu_B$ and $0.257 \mu_B$ magnetic moments emerge at the P^+ interface for the case with one V_{O3} and two V_{O3} (V_{O3} : oxygen vacancy in the third atomic layer), corresponding to a spin density of $\sigma^s = 5.95 \mu C/cm^2$ and $\sigma^s = 26.35 \mu C/cm^2$, respectively. The polarization P is defined as [32,33]

$$P = \frac{e}{\Omega} \sum_{m=1}^N Z_m^* \Delta_{Z_m}, \quad (2)$$

where Ω is the volume of unit cell, N is the number of atoms in the unit cell, and Z^* is the Born effective charge [34] (calculated Z^* for Pb: 3.30, Ti: 4.59, O_A : -3.99, O_B : -1.95 in $PbTiO_3$; Sr: 2.54, Ti: 7.82, O_A : -6.25, O_B : -2.05 in $SrTiO_3$, where O_A locates at Pb-O/Sr-O layers, and O_B locates at Ti-O layers). Here Δ_{Z_m} is the displacement of the m th atom away from its position in symmetric structure. We obtain that $\eta_{V_{O3}} = 0.12$ and $\eta_{2V_{O3}} = 0.51$ for V_O densities of 0.8% and 1.6% (one V_O and two V_O out of 120 oxygen atoms) in the $PbTiO_3/SrTiO_3$ heterostructure. The latter is much larger than the value $\eta = 0.37$ for the $BaTiO_3/SrRuO_3$ heterostructure [6]. As the density of V_O dominates the strength of magnetoelectric coupling, we could obtain a stronger magnetoelectric coupling by increasing the density of V_O . In addition, the distribution of V_O within the $SrTiO_3$ layers and the interactions between adjacent oxygen vacancies [35] have minor effects on the resulting magnetoelectric coupling. Only the results of V_O near the interface are shown as representative examples, since in practice only the $SrTiO_3$

layers near the interface are effectively polarized. Electrons from V_O near the interface are more easily driven to the interface to form 2DEG.

Apart from providing free electrons, however, the local crystalline distortions induced by V_O in $SrTiO_3$ obscure the analysis on the mechanism of magnetoelectric coupling. As shown in Figs. 1(b) and 2(b), locations of V_O are positively charged as extra electrons are driven away by the polarizing field. Due to their mutual Coulombic attraction, the surrounding negatively charged oxygen anions move toward the locations of V_O . Thus the local displacements between anions and cations can shrink to zero or even negative values. (Negative displacement means that the anion is at the left side of the cation, and the polarization becomes rightward.) As a result, ferroelectric domain walls are yielded near the interface of the heterostructure; meanwhile the local TiO_6 octahedra are tilted and rotated [26,36]. Accordingly, it is difficult to rule out the possibility of a domain-wall mechanism for electron accumulation which is similar to that in $PbTiO_3/LaAlO_3$ heterostructures [7]. Since the main role of V_O is to provide free electrons, an alternative strategy for increasing the density of charge carriers is to directly dope electrons into the intact $PbTiO_3/SrTiO_3$ heterostructure, mimicking the effect brought by the presence of oxygen vacancies and other donors far away from the interface. In this way, not only are the side effects of V_O to induce crystalline distortion avoided, but the electronic control of the system is also more convenient.

To look into the mechanism of magnetoelectric coupling, we dope 1–4 electrons to the $(PbTiO_3)_{1 \times 1 \times 7}/(SrTiO_3)_{1 \times 1 \times 7}$ heterostructure (corresponding to V_O concentrations of 1.2% to 4.8%), as shown in Fig. 3. The neutral case is also shown for comparison. We see that free electrons are accumulated at the P^+ interface, where the ferroelectric domain wall is absent. With the doping electrons increasing from 1 to 4, the interfacial magnetism increases from $0.204 \mu_B$ to $0.498 \mu_B$, and the magnetoelectric coupling η defined in Eq. (1) increases from 0.22 to 0.51. We note that the induced polarization in

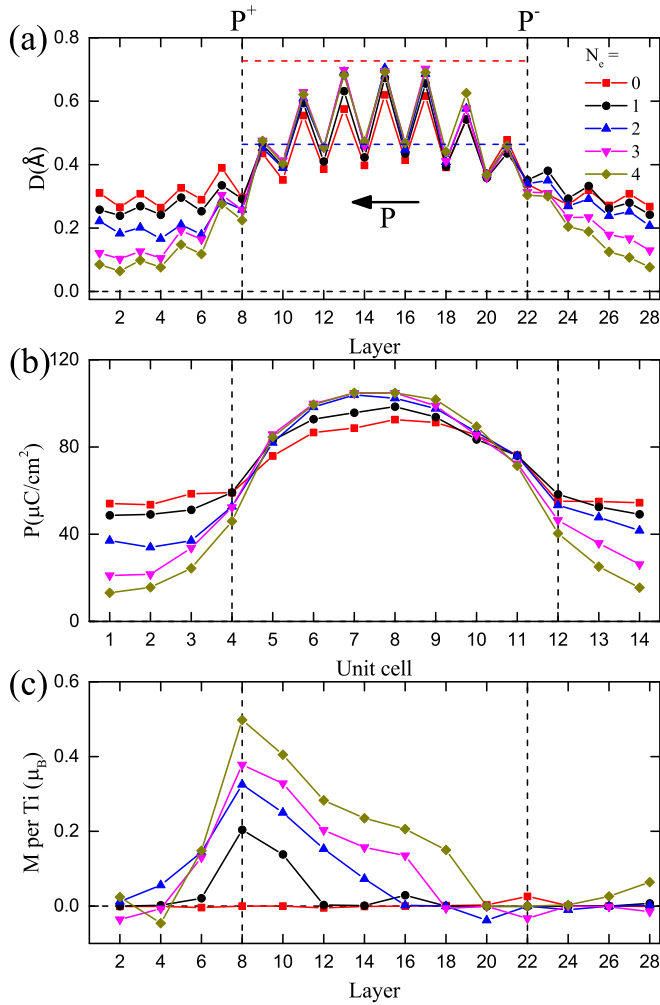


FIG. 3. (a) The local displacements between in-plane anions and cations for intact $(\text{PbTiO}_3)_{1 \times 1 \times 7}/(\text{SrTiO}_3)_{1 \times 1 \times 7}$. N_e is the number of electrons doped in the system. Polarization is initialized as leftward. Vertical dashed lines denote the Ti-O interfaces. Red and blue horizontal dashed lines are the displacements between in-plane anions and cations in bulk PbTiO_3 . (b) Polarization P defined by Eq. (2) calculated for each unit cell. (c) Layer-averaged magnetic moments per Ti atom in each Ti-O layer.

SrTiO_3 (e.g., the first unit cell) decreases from $48.7 \mu\text{C}/\text{cm}^2$ to $13.1 \mu\text{C}/\text{cm}^2$, approaching its value in bulk phase (having no polarization). The ferromagnetism and ferroelectricity-induced polarization show obvious competitive behaviors. Therefore we conclude that the 2DEG present at the interface partly screens out the polarization in PbTiO_3 and that the magnetoelectric coupling is 2DEG mediated. With more doped electrons, more Ti atoms adjacent to the interface become magnetic, indicating that the thickness of 2DEG becomes larger [Fig. 3(c)]. Given that the doped electrons accumulate at the interface and that our system is large enough (the thickness along z direction is about 60 \AA), the interaction between the charged system and the compensating homogeneous positive charge background applied automatically by VASP is very small and does not affect our conclusion.

Combining the results for doping V_O in $(\text{PbTiO}_3)_{2 \times 2 \times 5}/(\text{SrTiO}_3)_{2 \times 2 \times 5}$ and doping electrons in

$(\text{PbTiO}_3)_{1 \times 1 \times 7}/(\text{SrTiO}_3)_{1 \times 1 \times 7}$, we gain a clear picture about the 2DEG-mediated magnetoelectric coupling. Paraelectric SrTiO_3 is polarized by ferroelectric PbTiO_3 . When there is no V_O or doped electrons, there is no magnetism. Under the induced electric field in SrTiO_3 , extra electrons from V_O or other dopants are driven in the opposite direction of electric field to the $\text{PbTiO}_3/\text{SrTiO}_3$ interface and accumulated at the P^+ interface to form a 2DEG. Free electrons are captured by interfacial Ti atoms, and Ti atoms become ferromagnetic when the 2DEG density is high. The accumulated charges at the P^+ interface in turn screen and reduce the interface polarization, making SrTiO_3 approach the behavior of bulk phase. Thus the key reasons for the emergence of 2DEG and the ferromagnetism at the P^+ interface are the strong polarization field induced by ferroelectric PbTiO_3 and free screening electrons from dopants in SrTiO_3 .

The above discussion on the mechanism of a two-dimensional ferromagnetic conducting layer between two nonmagnetic insulators has ignored the least charges needed to screen polarization and to form ferromagnetism, and the effects of strain on magnetoelectric coupling [36,37]. The lower boundary of screening charges is determined by the sharp change in magnetic moment per Ti at the P^+ layer when more electrons are doped. As shown in Fig. 4(a), a phase transition occurs at the doping level of 0.5 electrons per unit-cell area when epitaxial strain is absent, equivalent to one V_O in $(\text{PbTiO}_3)_{2 \times 2 \times 5}/(\text{SrTiO}_3)_{2 \times 2 \times 5}$. The critical number of electrons is slightly decreased (increased) when the tensile (compressive) strain is applied. The tensile and compressive strain can be realized experimentally by depositing $\text{PbTiO}_3/\text{SrTiO}_3$ thin film on substrates with large lattice mismatches.

We obtain a phase diagram where the boundary between the nonmagnetic (NM) and ferromagnetic (FM) phase at the P^+ interface is a function of applied strain ε and accumulated charge density σ [Fig. 4(b)]. The critical charge density σ for the emergence of FM ordering is found to be $17.9 \mu\text{C}/\text{cm}^2$, $15.5 \mu\text{C}/\text{cm}^2$, and $14.1 \mu\text{C}/\text{cm}^2$ under the strain of -2% , 0% , and 2% , respectively. When the charge density reaches the critical value, the magnetic moment of Ti develops, and the exchange interaction between two adjacent Ti atoms via the bridging oxygen is strong enough to make Ti^{3+} forming ferromagnetic alignments. The corresponding spin density σ^s is $8.6 \mu\text{C}/\text{cm}^2$, $6.5 \mu\text{C}/\text{cm}^2$, and $5.9 \mu\text{C}/\text{cm}^2$ for -2% , 0% , and 2% strained films, respectively, implying about 40% of the electrons of the 2DEG is polarized. The proportion of polarized electrons gradually increases to 80% when the 2DEG density is further increased. The resulting magnetic moment per Ti reaches as high as $0.5 \mu_B$ and becomes saturated [Fig. 4(a)]. As the 2DEG density increases, the gradual increase in the fraction of polarized electrons and the magnetic moment results in a large magnetoelectric coupling. Comparing with $\text{PbTiO}_3/\text{LaAlO}_3$, where ferromagnetism comes from electrons doped by the charged LaO^+ interface layer, and $\text{BaTiO}_3/\text{SrRuO}_3$, where ferromagnetism comes from local Ru $4d$ electrons in ferromagnetic metal SrRuO_3 , $\text{PbTiO}_3/\text{SrTiO}_3$ possesses a strong magnetoelectric coupling strength as its magnetoelectric coupling is mediated by itinerant and high-density 2DEG, triggering its potential application in spintronics and information storage. The critical

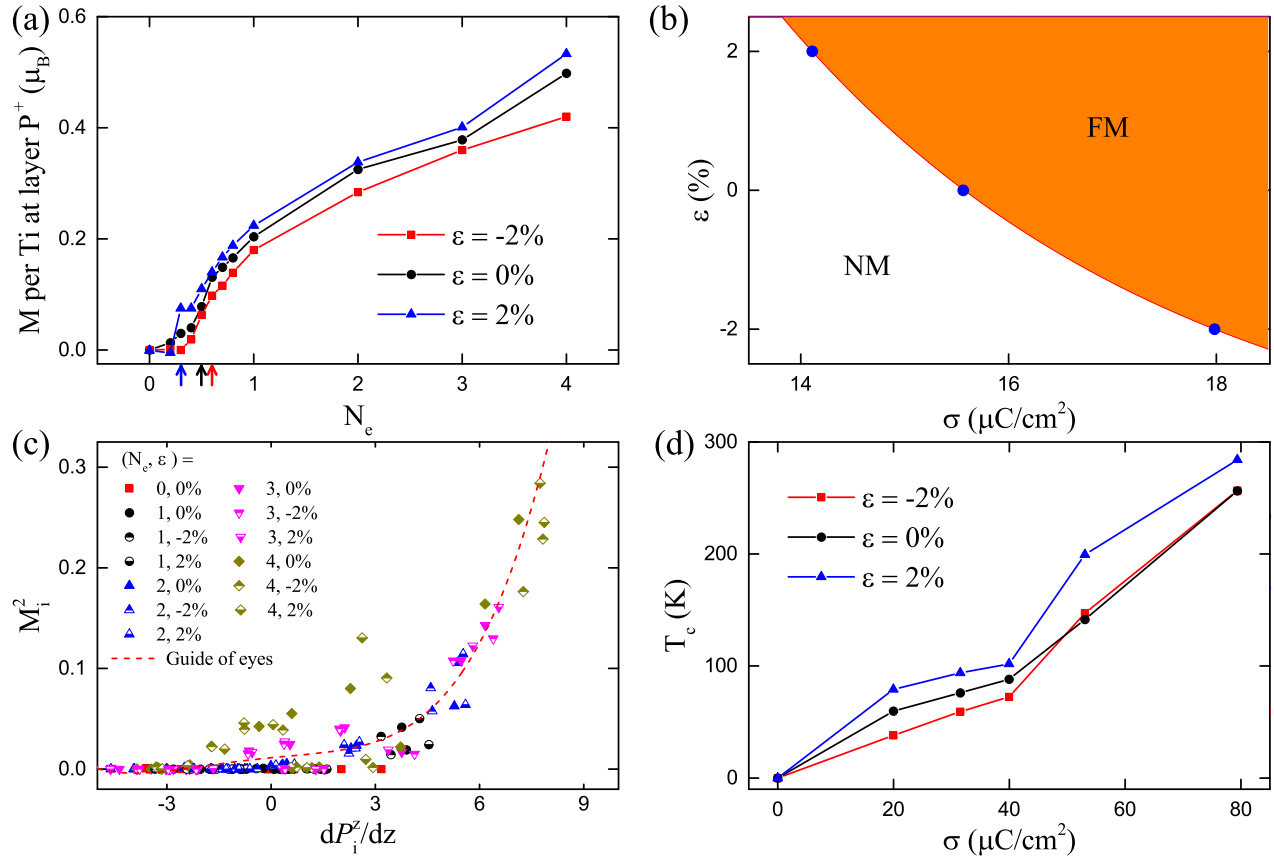


FIG. 4. Magnetoelectric properties for $(\text{PbTiO}_3)_{1 \times 1 \times 7}/(\text{SrTiO}_3)_{1 \times 1 \times 7}$. (a) Magnetic moments per Ti atom at the P^+ interface as a function of the number of doped electrons. Arrows denote the critical density for the abrupt emergence of ferromagnetism. (b) Phase diagram of interfacial nonmagnetism (NM) and ferromagnetism (FM) phases. The boundary is a function of the applied strain ε and the accumulated charge density σ at the P^+ interface. (c) The $(M_i^2, dP_i^z/dz)$ distributions with different number of doped electrons and strains. Here i is the unit-cell number; and M_i , P_z , and z are in units of μ_B , $\mu\text{C}/\text{cm}^2$, and \AA , respectively. The red dashed line is a guide for the eyes. (d) Curie temperatures T_C as a function of σ at the P^+ interface.

density to achieve ferromagnetism in strain-free film, $\sigma = 15.5 \mu\text{C}/\text{cm}^2$, is at least 3 times smaller than the critical charge density [8] of $52.5 \mu\text{C}/\text{cm}^2$ required to form 2DEG in $\text{LaAlO}_3/\text{SrTiO}_3$. This fact gives rise to the scientific and technological promise for effective magnetoelectric control.

The type of magnetoelectric coupling revealed in the present work belongs to the category of carrier driven [6,7]. In Fig. 3(b), the sharp change of polarization at the P^+ interface indicates a large positive dP_z/dz . Here dP_z/dz describes a net charge at position z [derived from Eq. (2)], and hence the discontinuity of ferroelectric polarization at the interface controls the interfacial magnetism, and this is the reason why free electrons are trapped at the P^+ layer. As ferromagnetism breaks the time-reversal symmetry, we consider $M^2(dP_z/dz)$ -type magnetoelectric coupling to restore the time- and space-reversal symmetry of energy, shown in Fig. 4(c). We find that a large M^2 is always accompanied with a large dP_z/dz in a wide range of values for doped electrons and applied strains. The calculated interfacial ferromagnetism is further enhanced using the GGA + U method, with $U = 6$ eV and $J = 0.7$ eV [38], indicating a possible stronger magnetoelectric coupling strength in practice.

The $\text{PbTiO}_3/\text{SrTiO}_3$ heterostructure as a magnetoelectric material can be operated at room temperature, provided that

sufficiently high anisotropy can be obtained. In the large- N limit, the Curie temperature T_C of two-dimensional magnetic order is calculated by the following equation [39,40]:

$$T_C = T_3 / \ln \left(\frac{3\pi T_3}{4 K} \right), \quad (3)$$

where K is the anisotropy constant assumed to be 60 K. $T_3 = 4\pi J/3$ is the Curie temperature of three-dimensional magnetic order. J is the strength of the exchange coupling given by the following equation:

$$J = \frac{E_{\text{AFM}} - E_{\text{FM}}}{zN_{\text{FM}}}, \quad (4)$$

where E_{AFM} and E_{FM} are the free energies of antiferromagnetic and ferromagnetic phases, N_{FM} is the number of atoms exhibiting magnetic moment in ferromagnetic material, and z is the coordination number. Here $z = 4$ and 6 for two-dimensional and three-dimensional magnetic order, respectively. In Fig. 4(d), T_C reaches room temperature when the accumulated interface charge density reaches $\sigma \approx 80 \mu\text{C}/\text{cm}^2$ (corresponding to six doped electrons in $(\text{PbTiO}_3)_{1 \times 1 \times 7}/(\text{SrTiO}_3)_{1 \times 1 \times 7}$; here $\sigma \sim \sigma^s$). We can acquire this critical charge density easily by increasing the density of V_O , applying tensile strain and/or external electric field in

practice, given that the tensile strain can enhance magnetism and therefore the T_C (Fig. 4). The density of 2DEG can also be enhanced when an external electric field parallel to the polarizing field of PbTiO_3 is applied. On the contrary, when an antiparallel electric field is applied, the polarizing field is reversed and eventually P^+ changes into P^- . Then electrons will be pushed back into SrTiO_3 , and the interface ferromagnetism and the magnetoelectric coupling diminishes.

We predict from extensive first-principles calculations the emergence of ferromagnetism at the ferroelectric $\text{PbTiO}_3/\text{SrTiO}_3$ heterostructure. The strong magnetoelectric coupling mediated by 2DEG enables a convenient control of magnetism by electric field and vice versa. Besides, the $\text{PbTiO}_3/\text{SrTiO}_3$ heterostructure is of particular interest

in spintronics and information storage compared to other magnetoelectric coupling materials, not only because it is cheaper, easily grown, and controllable, but also because it can be operated at room temperature with a reasonable doping level.

We acknowledge Dr. Z. H. Ren and Dr. H. Tian for introducing us to this topic and helpful discussion. This work was supported by the National Key Basic Research Program of China (Grants No. 2016YFA0300902 and No. 2015CB921001), the National Natural Science Foundation of China (Grant No. 11474328), and the Strategic Priority Research Program (B) of the Chinese Academy of Sciences (Grant No. XDB07030100).

-
- [1] K. O'Grady and H. Laidler, *J. Magn. Magn. Mater.* **200**, 616 (1999).
- [2] W. Eerenstein, N. D. Mathur, and J. F. Scott, *Nature (London)* **442**, 759 (2006).
- [3] T. Shimada, Y. Uratani, and T. Kitamura, *Appl. Phys. Lett.* **100**, 162901 (2012).
- [4] N. A. Hill, *J. Phys. Chem. B* **104**, 6694 (2000).
- [5] J. F. Scott, *Science* **315**, 954 (2007).
- [6] J. M. Rondinelli, M. Stengel, and N. A. Spaldin, *Nat. Nanotechnol.* **3**, 46 (2008).
- [7] P. X. Zhou, S. Dong, H. M. Liu, C. Y. Ma, Z. B. Yan, C. G. Zhong, and J.-M. Liu, *Sci. Rep.* **5**, 13052 (2015).
- [8] A. Ohtomo and H. Y. Hwang, *Nature (London)* **427**, 423 (2004).
- [9] G. Herranz, M. Basletić, M. Bibes, C. Carrétéro, E. Tafrá, E. Jacquet, K. Bouzehouane, C. Deranlot, A. Hamzić, J.-M. Broto *et al.*, *Phys. Rev. Lett.* **98**, 216803 (2007).
- [10] K. Yoshimatsu, R. Yasuhara, H. Kumigashira, and M. Oshima, *Phys. Rev. Lett.* **101**, 026802 (2008).
- [11] M. K. Niranjan, Y. Wang, S. S. Jaswal, and E. Y. Tsymlal, *Phys. Rev. Lett.* **103**, 016804 (2009).
- [12] Z. Zhang, P. Wu, L. Chen, and J. Wang, *Appl. Phys. Lett.* **99**, 062902 (2011).
- [13] L. Li, C. Richter, J. Mannhart, and R. C. Ashoori, *Nat. Phys.* **7**, 762 (2011).
- [14] M. R. Fitzsimmons, N. W. Hengartner, S. Singh, M. Zhernenkov, F. Y. Bruno, J. Santamaria, A. Brinkman, M. Huijben, H. J. A. Molegraaf, J. de La Venta *et al.*, *Phys. Rev. Lett.* **107**, 217201 (2011).
- [15] F. Bi, M. Huang, S. Ryu, H. Lee, C.-W. Bark, C.-B. Eom, P. Irvin, and J. Levy, *Nat. Commun.* **5**, 5019 (2014).
- [16] G. Kresse and J. Furthmüller, *Phys. Rev. B* **54**, 11169 (1996).
- [17] J. P. Perdew, K. Burke, and M. Ernzerhof, *Phys. Rev. Lett.* **77**, 3865 (1996).
- [18] G. Kresse and D. Joubert, *Phys. Rev. B* **59**, 1758 (1999).
- [19] B. Meyer and D. Vanderbilt, *Phys. Rev. B* **63**, 205426 (2001).
- [20] D. D. Fong, G. B. Stephenson, S. K. Streiffer, J. A. Eastman, O. Auciello, P. H. Fuoss, and C. Thompson, *Science* **304**, 1650 (2004).
- [21] M. Dawber, K. M. Rabe, and J. F. Scott, *Rev. Mod. Phys.* **77**, 1083 (2005).
- [22] P. Aguado-Puente and J. Junquera, *Phys. Rev. B* **85**, 184105 (2012).
- [23] B. Yin and S. Qu, *J. Appl. Phys.* **114**, 063703 (2013).
- [24] D. Lee, H. Lu, Y. Gu, S.-Y. Choi, S.-D. Li, S. Ryu, T. R. Paudel, K. Song, E. Mikheev, S. Lee *et al.*, *Science* **349**, 1314 (2015).
- [25] B. Yin, P. Aguado-Puente, S. Qu, and E. Artacho, *Phys. Rev. B* **92**, 115406 (2015).
- [26] P. Aguado-Puente, P. Garcia-Fernandez, and J. Junquera, *Phys. Rev. Lett.* **107**, 217601 (2011).
- [27] W. Gong, H. Yun, Y. Ning, J. Greedan, W. Datars, and C. Stager, *J. Solid State Chem.* **90**, 320 (1991).
- [28] A. Samanta, W. N. E, and S. B. Zhang, *Phys. Rev. B* **86**, 195107 (2012).
- [29] W. Luo, W. Duan, S. G. Louie, and M. L. Cohen, *Phys. Rev. B* **70**, 214109 (2004).
- [30] Y. Zhang, J. Hu, E. Cao, L. Sun, and H. Qin, *J. Magn. Magn. Mater.* **324**, 1770 (2012).
- [31] W. Rice, P. Ambwani, M. Bombeck, J. Thompson, G. Haugstad, C. Leighton, and S. Crooker, *Nat. Mater.* **13**, 481 (2014).
- [32] P.-Z. Wang, T.-Y. Cai, S. Ju, and Y.-Z. Wu, *Sci. Rep.* **6**, 24209 (2016).
- [33] T. Cai, S. Ju, J. Lee, N. Sai, A. A. Demkov, Q. Niu, Z. Li, J. Shi, and E. Wang, *Phys. Rev. B* **80**, 140415 (2009).
- [34] R. M. Pick, M. H. Cohen, and R. M. Martin, *Phys. Rev. B* **1**, 910 (1970).
- [35] D. D. Cuong, B. Lee, K. M. Choi, H.-S. Ahn, S. Han, and J. Lee, *Phys. Rev. Lett.* **98**, 115503 (2007).
- [36] M. Li, J. Li, L.-Q. Chen, B.-L. Gu, and W. Duan, *Phys. Rev. B* **92**, 115435 (2015).
- [37] C. Ederer and N. A. Spaldin, *Phys. Rev. Lett.* **95**, 257601 (2005).
- [38] K. Rahmanizadeh, D. Wortmann, G. Bihlmayer, and S. Blügel, *Phys. Rev. B* **90**, 115104 (2014).
- [39] R. Grau-Crespo, N. H. de Leeuw, and C. R. A. Catlow, *J. Mater. Chem.* **13**, 2848 (2003).
- [40] M. Bander and D. L. Mills, *Phys. Rev. B* **38**, 12015(R) (1988).